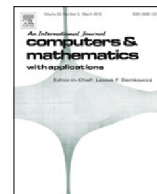




Contents lists available at ScienceDirect

## Computers and Mathematics with Applications

journal homepage: [www.elsevier.com/locate/camwa](http://www.elsevier.com/locate/camwa)

# Mass-conservative Fourier spectral methods for solving the fractional nonlinear Schrödinger equation<sup>☆</sup>

Siwei Duo, Yanzhi Zhang<sup>\*</sup>

Department of Mathematics and Statistics, Missouri University of Science and Technology, Rolla, MO 65409-0020, USA

## ARTICLE INFO

## Article history:

Available online 3 February 2016

## Keywords:

Fractional nonlinear Schrödinger equation  
 Fractional Laplacian  
 Split-step method  
 Crank–Nicolson method  
 Relaxation method

## ABSTRACT

We propose three Fourier spectral methods, i.e., the split-step Fourier spectral (SSFS), the Crank–Nicolson Fourier spectral (CNFS), and the relaxation Fourier spectral (ReFS) methods, for solving the fractional nonlinear Schrödinger (NLS) equation. All of them are mass conservative and time reversible, and they have the spectral order accuracy in space and the second-order accuracy in time. In addition, the CNFS and ReFS methods are energy conservative. The performance of these methods in simulating the plane wave and soliton dynamics is discussed. The SSFS method preserves the dispersion relation, and thus it is more accurate for studying the long-time behaviors of the plane wave solutions. Furthermore, our numerical simulations suggest that the SSFS method is better in solving the defocusing NLS, but the CNFS and ReFS methods are more effective for the focusing NLS.

© 2016 Elsevier Ltd. All rights reserved.

## 1. Introduction

The fractional Schrödinger equation is a nonlocal dispersive equation, which was first introduced in [1,2] by generalizing the Feynman path integral over Lévy trajectories. Recently, it has also been derived as the continuum limit of a microscopic lattice system with long-range interactions [3]. The nonlocality of the fractional Schrödinger equation enables it to describe new phenomena which are absent from the standard Schrödinger equation [4–7]. However, the nonlocality also introduces considerable challenges in finding the solutions of the fractional Schrödinger equation. Hence, the understanding of its solutions still remains limited. In this paper, we propose three mass-conservative Fourier spectral methods for numerically solving the fractional nonlinear Schrödinger (NLS) equation, and the performance of these methods is examined and compared both analytically and numerically.

We consider the fractional nonlinear Schrödinger (NLS) equation in the semiclassical regime [8–10]:

$$i\varepsilon \frac{\partial u(\mathbf{x}, t)}{\partial t} = \varepsilon^\alpha (-\Delta)^{\alpha/2} u(\mathbf{x}, t) + \beta |u(\mathbf{x}, t)|^{2\sigma} u(\mathbf{x}, t), \quad t > 0, \quad (1.1)$$

$$u(\mathbf{x}, 0) = \psi(\mathbf{x}), \quad (1.2)$$

where  $i = \sqrt{-1}$ , and  $u(\mathbf{x}, t)$  is a complex-valued wave function of  $\mathbf{x} \in \mathbb{R}^d$  (for  $d = 1, 2$ , or  $3$ ) and  $t \geq 0$ .  $0 < \varepsilon \leq 1$  is a small semiclassical parameter, and the constant  $\sigma > 0$ . The parameter  $\beta \in \mathbb{R}$  describes the strength of short-range (or

<sup>☆</sup> This research was supported by the National Science Foundation grant DMS-1217000.

<sup>\*</sup> Corresponding author.

E-mail addresses: [sddy9@mst.edu](mailto:sddy9@mst.edu) (S. Duo), [zhangyanz@mst.edu](mailto:zhangyanz@mst.edu) (Y. Zhang).

local) nonlinear interactions; if  $\beta$  is positive (resp. negative), the interactions are repulsive or defocusing (resp. attractive or focusing). The fractional Laplacian  $(-\Delta)^{\alpha/2}$  is defined via a pseudo-differential operator [11–14]:

$$(-\Delta)^{\alpha/2}u(\mathbf{x}) := \mathcal{F}^{-1}[-|\xi|^\alpha \mathcal{F}[u]], \quad \alpha > 0, \tag{1.3}$$

where  $\mathcal{F}$  represents the Fourier transform, and  $\mathcal{F}^{-1}$  denotes its inverse. If  $\alpha = 2$ , the fractional Laplacian in (1.3) reduces to the standard Laplace operator, but for  $\alpha \in (0, 2)$ , it is a nonlocal operator describing long-range interactions [11,3,15].

Similar to the standard ( $\alpha = 2$ ) NLS, the fractional NLS (1.1) has two important conserved quantities: the mass of the wave function:

$$N(t) = \|u(\cdot, t)\|^2 := \int_{\mathbb{R}^d} |u(\mathbf{x}, t)|^2 d\mathbf{x} \equiv N(0), \tag{1.4}$$

and the total energy (or Hamiltonian):

$$E(t) = \int_{\mathbb{R}^d} \left[ \varepsilon^\alpha \operatorname{Re} \left( u^*(\mathbf{x}, t) (-\Delta)^{\alpha/2} u(\mathbf{x}, t) \right) + \frac{\beta}{\sigma + 1} |u(\mathbf{x}, t)|^{2(\sigma+1)} \right] d\mathbf{x} \equiv E(0), \tag{1.5}$$

where  $\operatorname{Re}(\phi)$  and  $\phi^*$ , respectively, represent the real part and the complex conjugate of a function  $\phi$ . The fractional NLS is time reversible, that is, (1.1) remains invariant if one replaces the time  $t$  by  $-t$  and takes its conjugate. These properties are usually used as benchmarks to develop and examine numerical methods for the fractional NLS.

The fractional NLS (1.1) admits the plane wave solution of the form:

$$u(\mathbf{x}, t) = A \exp[i(\boldsymbol{\lambda}_k \cdot \mathbf{x} - \omega t)], \tag{1.6}$$

provided that the dispersion relation

$$\omega = \varepsilon^{\alpha-1} |\boldsymbol{\lambda}_k|^\alpha + \frac{\beta}{\varepsilon} |A|^{2\sigma}, \tag{1.7}$$

is satisfied. Here,  $A$  is the amplitude of the plane wave solution,  $\boldsymbol{\lambda}_k \in \mathbb{R}^d$  is the vector of wave numbers, and  $\omega$  is the time frequency. It shows in [15] that due to its nonlocality, the stability and dynamics of the plane wave solutions in the fractional NLS are significantly different from those in the standard NLS. In numerical studies of plane wave dynamics, it is desirable for a numerical method to preserve the dispersion relation in (1.7).

Both the nonlocality and nonlinearity of the fractional NLS make it extremely challenging to find its analytical solutions. Therefore, numerical simulations play an important role in the study of the fractional NLS. However, in contrast to the standard NLS, only a few numerical methods are available in the literature for solving the fractional NLS. For example, a second-order finite difference method is proposed in [16,17], which is based on the fractional centered difference discretization of the Riesz fractional derivatives. In [18], collocation methods are presented to solve the fractional linear Schrödinger equation. Recently, a split-step Fourier spectral method is applied in [19] to study the decoherence of solitons in the fractional Schrödinger equation, but the properties of this method are not discussed. In this paper, we aim to develop accurate numerical methods for solving the fractional NLS, which preserve one or more analytical properties of the fractional NLS, including mass conservation, energy conservation, time reversible, and dispersion relation. In addition, some remarks are provided for numerical simulations of the fractional NLS.

The paper is organized as follows. In Section 2, we introduce three methods for solving the fractional NLS, and the properties of these methods are analyzed in detail. Numerical examples are presented in Section 3 to examine and compare the performance of our numerical methods in solving the fractional NLS. Some concluding remarks are made in Section 4.

## 2. Numerical methods

In this section, we introduce three Fourier spectral methods for solving the fractional NLS (1.1)–(1.2) and prove that all of them are mass conservative in the discrete level. Some other properties, such as energy conservation, time reversible, and dispersion relation, are also discussed for each method. For simplicity of notation, we will introduce our numerical methods for the one-dimensional (i.e.,  $d = 1$ ) fractional NLS. The generalization of these methods to higher dimensions is straightforward. First, we truncate (1.1)–(1.2) into a finite computational domain  $[-L, L]$  with periodic boundary conditions and consider the following problem:

$$i\varepsilon \partial_t u(x, t) = \varepsilon^\alpha (-\Delta)^{\alpha/2} u(x, t) + \beta |u(x, t)|^{2\sigma} u(x, t), \quad t > 0, \tag{2.1}$$

$$u(x, 0) = \psi(x), \tag{2.2}$$

for  $x \in [-L, L]$ . We usually choose  $L$  to be sufficiently large, unless plane wave solutions are studied [15]. We will leave the discussion of other boundary conditions for our future work.

Let  $\tau > 0$  denote a time step, and define the time sequence  $t_n = n\tau$  for  $n \geq 0$ . Define the mesh size  $h = 2L/J$ , with  $J$  a positive even integer. Denote spatial grid points  $x_j = -L + jh$ , for  $0 \leq j \leq J$ . Let  $u_j^n$  be the numerical approximation of the solution  $u(x_j, t_n)$ . Then, we denote the solution vector at time  $t = t_n$  as  $U^n = (u_0^n, u_1^n, \dots, u_{J-1}^n)^T$ . Due to the definition of

fractional Laplacian in (1.3), it is natural to use the Fourier spectral method for spatial discretization. Hence, we assume the ansatz:

$$u(x, t) = \sum_{l=-J/2}^{J/2-1} \widehat{u}_l(t) \exp(i\mu_l x), \tag{2.3}$$

where  $\mu_l = l\pi/L$ , for  $-J/2 \leq l \leq J/2 - 1$ . In the following, we will focus on the temporal discretization and the properties of the resulting numerical methods.

2.1. Split-step Fourier spectral method

The split-step method, also known as the time-splitting method, is one of the most popular numerical methods for solving the standard NLS (also known as the Gross–Pitaevskii equation in the literature of Bose–Einstein condensation [20–22]). It is an explicit method and thus avoids solving nonlinear systems at each time step. The main idea of this method is outlined below. From time  $t = t_n$  to  $t = t_{n+1}$ , the fractional NLS (2.1) is solved in two steps:

$$i\varepsilon u_t(x, t) = \beta |u(x, t)|^{2\sigma} u(x, t), \tag{2.4}$$

$$i\varepsilon u_t(x, t) = \varepsilon^\alpha (-\Delta)^{\alpha/2} u(x, t). \tag{2.5}$$

On one hand, multiplying  $u^*(x, t)$  at both sides of (2.4) and subtracting it from its conjugate, we obtain that  $|u(x, t)| = |u(x, t_n)|$  for any  $t \in [t_n, t_{n+1}]$ . Therefore, (2.4) reduces to

$$i\varepsilon u_t(x, t) = \beta |u(x, t_n)|^{2\sigma} u(x, t).$$

Integrating it in time yields the solution to (2.4):

$$u(x, t) = u(x, t_n) \exp[-i\beta |u(x, t_n)|^{2\sigma} (t - t_n)/\varepsilon], \quad t \in [t_n, t_{n+1}]. \tag{2.6}$$

On the other hand, substituting (2.3) into (2.5), we obtain that

$$i \frac{d\widehat{u}_l(t)}{dt} = \varepsilon^{\alpha-1} |\mu_l|^\alpha \widehat{u}_l(t), \quad -\frac{J}{2} \leq l \leq \frac{J}{2} - 1.$$

Integrating it in time gives

$$\widehat{u}_l(t) = \widehat{u}_l(t_n) \exp[-i\varepsilon^{\alpha-1} |\mu_l|^\alpha (t - t_n)], \quad t \in [t_n, t_{n+1}] \tag{2.7}$$

for  $-J/2 \leq l \leq J/2 - 1$ . Combining (2.3) and (2.7) gives the numerical approximation to the solution of (2.5).

In practice, we can combine the steps (2.4) and (2.5) by the second order Strang splitting method, resulting in the second-order split-step Fourier spectral (SSFS) method for the fractional NLS (2.1)–(2.2) as follows:

$$u_j^{n,1} = u_j^n \exp(-i\beta \tau |u_j^n|^{2\sigma} / 2\varepsilon), \tag{2.8}$$

$$u_j^{n,2} = \sum_{l=-J/2}^{J/2-1} \widehat{u}_l^{n,1} \exp(-i\varepsilon^{\alpha-1} |\mu_l|^\alpha \tau) \exp(i\mu_l x_j), \tag{2.9}$$

$$u_j^{n+1} = u_j^{n,2} \exp(-i\beta \tau |u_j^{n,2}|^{2\sigma} / 2\varepsilon), \tag{2.10}$$

for  $0 \leq j \leq J - 1$  and  $n \geq 0$ , where  $\widehat{u}_l^{n,1}$  (for  $-J/2 \leq l \leq J/2 - 1$ ) is the  $l$ th discrete Fourier transform coefficient of the vector solution  $U^{n,1}$ . The initial condition (2.2) is discretized as:

$$u_j^0 = \psi(x_j), \quad 0 \leq j \leq J. \tag{2.11}$$

The SSFS method in (2.8)–(2.11) has the spectral order spatial accuracy and the second-order temporal accuracy, which can be efficiently implemented by the fast Fourier transform (FFT). Also, its temporal accuracy can be further improved by using a higher order split-step method [21].

It is easy to verify that the SSFS method (2.8)–(2.11) is time reversible, i.e., the method remains unchanged if  $\tau \leftrightarrow -\tau$  and  $n \leftrightarrow n + 1$ . Moreover, the SSFS method has the following properties:

**Lemma 2.1** (SSFS: Mass Conservation). *Suppose that  $U^n$  is the numerical solution of the fractional NLS at time  $t_n$ , obtained from the SSFS method in (2.8)–(2.11). Then, we have the discrete mass:*

$$N^n = h \sum_{j=0}^{J-1} |u_j^n|^2 = h \sum_{j=0}^{J-1} |u_j^0|^2 \equiv N^0, \quad n \geq 0, \tag{2.12}$$

i.e., the mass is conserved at any time  $t_n$ .

**Proof.** From (2.9), we obtain that

$$\begin{aligned} \sum_{j=0}^{J-1} |u_j^{n,2}|^2 &= \sum_{j=0}^{J-1} \left| \sum_{l=-J/2}^{J/2-1} \widehat{u}_l^{n,1} \exp(-i\varepsilon^{\alpha-1} |\mu_l|^\alpha \tau) \exp(i\mu_l x_j) \right|^2 \\ &= \sum_{l,s=-J/2}^{J/2-1} \widehat{u}_l^{n,1} (\widehat{u}_s^{n,1})^* \exp[-i\varepsilon^{\alpha-1} \tau (|\mu_l|^\alpha - |\mu_s|^\alpha)] \sum_{j=0}^{J-1} \exp[i(\mu_l - \mu_s)x_j] \\ &= J \sum_{l=-J/2}^{J/2-1} |\widehat{u}_l^{n,1}|^2. \end{aligned} \tag{2.13}$$

By the discrete Parseval’s relation

$$\sum_{l=-J/2}^{J/2-1} |\widehat{u}_l^{n,1}|^2 = \frac{h}{2L} \sum_{j=0}^{J-1} |u_j^{n,1}|^2 = \frac{1}{J} \sum_{j=0}^{J-1} |u_j^{n,1}|^2,$$

we obtain from (2.8), (2.10) and (2.13) that

$$N^{n+1} = h \sum_{j=0}^{J-1} |u_j^{n+1}|^2 = h \sum_{j=0}^{J-1} |u_j^{n,2}|^2 = h \sum_{j=0}^{J-1} |u_j^{n,1}|^2 = h \sum_{j=0}^{J-1} |u_j^n|^2 = N^n,$$

which implies the mass conservation in (2.12), as  $n \geq 0$  is arbitrary.  $\square$

**Lemma 2.2** (SSFS: Dispersion Relation). *The SSFS method (2.8)–(2.11) preserves the dispersion relation  $\omega = \varepsilon^{\alpha-1} |\lambda_k|^\alpha + \beta |A|^{2\sigma} / \varepsilon$  of the plane wave solution of the fractional NLS.*

**Proof.** Assume that at  $t = t_n$  (for any  $n \geq 0$ ), the solution  $u_j^n$  has the form:

$$u_j^n = A \exp[i(\lambda_k x_j - \omega t_n)], \quad \text{with } \lambda_k = k\pi/L, \text{ for } k \in \mathbb{Z}. \tag{2.14}$$

Note that the wave number  $\lambda_k = \mu_k$ . On the one hand, from (2.14) and the solution  $u_j^{n,1}$  in (2.8), we get that

$$\widehat{u}_l^{n,1} = \begin{cases} 0, & \text{if } l \neq k, \\ A \exp(-i\omega t_n) \exp(-i\beta\tau |A|^{2\sigma} / 2\varepsilon), & \text{if } l = k, \end{cases}$$

for  $-J/2 \leq l \leq J/2 - 1$ . Plugging  $\widehat{u}_l^{n,1}$  into (2.9) and simplifying it, we get

$$u_j^{n,2} = u_j^n \exp(-i\beta\tau |A|^{2\sigma} / 2\varepsilon) \exp(-i\varepsilon^{\alpha-1} |\mu_k|^\alpha \tau).$$

Substituting the above solution  $u_j^{n,2}$  into (2.10), we get

$$u_j^{n+1} = u_j^n \exp[-i\tau (\varepsilon^{\alpha-1} |\mu_k|^\alpha + \beta |A|^{2\sigma} / \varepsilon)]. \tag{2.15}$$

On the other hand, setting  $n = n + 1$  in (2.14), we get

$$u_j^{n+1} = A \exp[i(\lambda_k x_j - \omega t_{n+1})] = u_j^n \exp(-i\omega\tau). \tag{2.16}$$

Comparing (2.15) and (2.16), we obtain

$$\omega = \varepsilon^{\alpha-1} |\lambda_k|^\alpha + \frac{\beta}{\varepsilon} |A|^{2\sigma},$$

i.e., the numerical solution from the SSFS method satisfies the dispersion relation of the plane wave solution.  $\square$

Lemma 2.2 implies that the SSFS method can exactly solve the plane wave solution of the NLS, if there is no numerical error, which makes it an ideal method to study the long-time behavior of the plane wave dynamics. However, the SSFS method, as an explicit method, is conditionally stable in simulating the plane wave solution, and one sufficient condition to avoid its numerical instability is that  $\tau < h^\alpha / \pi^{\alpha-1}$ , for  $\alpha \in (0, 2]$ . More discussion on the numerical stability of the SSFS method for the plane wave solutions can be found in [23,15].

2.2. Crank–Nicolson Fourier spectral method

In this section, we study the Crank–Nicolson Fourier spectral method for solving the fractional NLS. First, let us define the pseudo-differential operator

$$\delta_x^\alpha U^n \Big|_j = \sum_{l=-J/2}^{J/2-1} |\mu_l|^\alpha \widehat{u}_l^n \exp(i\mu_l x_j) \tag{2.17}$$

as a numerical approximation of  $(-\Delta)^{\alpha/2} u(x_j, t_n)$ , where  $\widehat{u}_l^n$  is the  $l$ th discrete Fourier transform coefficient of  $U^n$ .

Then, the Crank–Nicolson Fourier spectral (CNFS) method for the fractional NLS (2.1) reads:

$$i\varepsilon \frac{u_j^{n+1} - u_j^n}{\tau} = \frac{\varepsilon^\alpha}{2} (\delta_x^\alpha U^{n+1} \Big|_j + \delta_x^\alpha U^n \Big|_j) + \frac{\beta}{2} F(|u_j^{n+1}|^2, |u_j^n|^2)(u_j^{n+1} + u_j^n), \tag{2.18}$$

for  $0 \leq j \leq J - 1$  and  $n \geq 0$ , where the function  $F$  is defined as

$$F(\phi_1, \phi_2) = \int_0^1 (\theta\phi_1 + (1 - \theta)\phi_2)^\sigma d\theta.$$

It is easy to compute that

$$F(\phi_1, \phi_2) = \begin{cases} \phi_1^\sigma, & \text{if } \phi_1 = \phi_2, \\ \frac{1}{\sigma + 1} \cdot \frac{\phi_1^{\sigma+1} - \phi_2^{\sigma+1}}{\phi_1 - \phi_2}, & \text{if } \phi_1 \neq \phi_2. \end{cases}$$

At  $n = 0$ , the initial condition (2.2) is discretized as:

$$u_j^0 = \psi(x_j), \quad 0 \leq j \leq J. \tag{2.19}$$

The CNFS method (2.18)–(2.19) is an implicit scheme, which requires solving a nonlinear system at each time step. Hence, the computational cost of the CNFS method is higher than that of the SSFS method. However, the CNFS method conserves not only the mass but also the energy of the fractional NLS. In addition, the CNFS method is time reversible.

**Lemma 2.3** (CNFS: Mass Conservation). *Suppose that  $U^n$  is the numerical solution of the fractional NLS at time  $t_n$ , obtained from the CNFS method in (2.18)–(2.19). Then, we have the discrete mass*

$$N^n = h \sum_{j=0}^{J-1} |u_j^n|^2 = h \sum_{j=0}^{J-1} |u_j^0|^2 \equiv N^0, \quad n \geq 0. \tag{2.20}$$

**Proof.** Multiplying  $(u_j^{n+1} + u_j^n)^*$  to (2.18) and summing it up for  $0 \leq j \leq J - 1$ , we obtain

$$\begin{aligned} i\varepsilon \sum_{j=0}^{J-1} (u_j^{n+1} - u_j^n)(u_j^{n+1} + u_j^n)^* &= \sum_{j=0}^{J-1} \left( \frac{\beta}{2} F(|u_j^{n+1}|^2, |u_j^n|^2) |u_j^{n+1} + u_j^n|^2 \right. \\ &\quad \left. + \frac{\varepsilon^\alpha (u_j^{n+1} + u_j^n)^*}{2} \sum_{l=-J/2}^{J/2-1} |\mu_l|^\alpha (\widehat{u}_l^n + \widehat{u}_l^{n+1}) \exp(i\mu_l x_j) \right). \end{aligned} \tag{2.21}$$

Note that

$$\sum_{j=0}^{J-1} (u_j^{n+1} + u_j^n)^* \sum_{l=-J/2}^{J/2-1} |\mu_l|^\alpha (\widehat{u}_l^n + \widehat{u}_l^{n+1}) e^{i\mu_l x_j} = J \sum_{l=-J/2}^{J/2-1} |\mu_l|^\alpha |\widehat{u}_l^n + \widehat{u}_l^{n+1}|^2. \tag{2.22}$$

Taking the imaginary part of (2.21) and noticing that  $\varepsilon, \tau > 0$ , we get

$$\sum_{j=0}^{J-1} (|u_j^{n+1}|^2 - |u_j^n|^2) = 0,$$

which implies that  $N^{n+1} = N^n$  and thus (2.20), as  $n \geq 0$  is arbitrary.  $\square$

**Lemma 2.4** (CNFS: Energy Conservation). Suppose that  $U^n$  is the numerical solution of the fractional NLS at time  $t_n$ , obtained from the CNFS method in (2.18)–(2.19). Then, we have the discrete energy

$$E^n = h \sum_{j=0}^{J-1} \left[ \varepsilon^\alpha \sum_{l=-J/2}^{J/2-1} |\mu_l|^\alpha |\widehat{u}_l^n|^2 + \frac{\beta}{\sigma + 1} |u_j^n|^{2(\sigma+1)} \right] \equiv E^0, \quad n \geq 0. \tag{2.23}$$

**Proof.** Assume that  $|u_j^{n+1}| \neq |u_j^n|$  for any  $j$ . Multiplying  $(u_j^{n+1} - u_j^n)^*$  to (2.18) and summing it up for  $0 \leq j \leq J - 1$ , we get

$$\begin{aligned} i \frac{\varepsilon}{\tau} \sum_{j=0}^{J-1} |u_j^{n+1} - u_j^n|^2 &= \sum_{j=0}^{J-1} \left( \frac{\varepsilon^\alpha (u_j^{n+1} - u_j^n)^*}{2} \sum_{l=-J/2}^{J/2-1} |\mu_l|^\alpha (\widehat{u}_l^n + \widehat{u}_l^{n+1}) e^{i\mu_l x_j} \right. \\ &\quad \left. + \frac{\beta}{2(\sigma + 1)} \frac{|u_j^{n+1}|^{2(\sigma+1)} - |u_j^n|^{2(\sigma+1)}}{|u_j^{n+1}|^2 - |u_j^n|^2} (u_j^{n+1} + u_j^n)(u_j^{n+1} - u_j^n)^* \right). \end{aligned} \tag{2.24}$$

Note that

$$\sum_{j=0}^{J-1} (u_j^{n+1} - u_j^n)^* \sum_{l=-J/2}^{J/2-1} |\mu_l|^\alpha (\widehat{u}_l^n + \widehat{u}_l^{n+1}) e^{i\mu_l x_j} = \sum_{j=0}^{J-1} \sum_{l=-J/2}^{J/2-1} |\mu_l|^\alpha [ (|\widehat{u}_l^{n+1}|^2 - |\widehat{u}_l^n|^2) + 2i \operatorname{Im}(\widehat{u}_l^{n+1} \widehat{u}_l^n^*) ].$$

Taking the real part of (2.24) yields

$$\sum_{j=0}^{J-1} \left( \frac{\varepsilon^\alpha}{2} \sum_{l=-J/2}^{J/2-1} |\mu_l|^\alpha (|\widehat{u}_l^{n+1}|^2 - |\widehat{u}_l^n|^2) + \frac{\beta (|u_j^{n+1}|^{2(\sigma+1)} - |u_j^n|^{2(\sigma+1)})}{2(\sigma + 1)} \right) = 0.$$

Hence, we get

$$\sum_{j=0}^{J-1} \left[ \varepsilon^\alpha \sum_{l=-J/2}^{J/2-1} |\mu_l|^\alpha |\widehat{u}_l^{n+1}|^2 + \frac{\beta}{\sigma + 1} |u_j^{n+1}|^{2(\sigma+1)} \right] = \sum_{j=0}^{J-1} \left[ \varepsilon^\alpha \sum_{l=-J/2}^{J/2-1} |\mu_l|^\alpha |\widehat{u}_l^n|^2 + \frac{\beta}{\sigma + 1} |u_j^n|^{2(\sigma+1)} \right],$$

for any  $n \geq 0$ , which implies  $E^{n+1} = E^n$  and thus the energy conservation in (2.23).  $\square$

Assume that at time  $t = t_n$  (for any  $n \geq 0$ ), the solution  $u_j^n$  is a plane wave solution of the form in (2.14). Then, the time frequency  $\omega$  obtained from the CNFS method (2.18)–(2.19) satisfies the relation:

$$\tan \frac{\omega \tau}{2} = \frac{\tau}{2} \left( \varepsilon^{\alpha-1} |\lambda_k|^\alpha + \frac{\beta}{\varepsilon} |A|^{2\sigma} \right). \tag{2.25}$$

If  $\omega \tau \ll 1$ , the Taylor expansion of (2.25) yields

$$\omega = \left( \varepsilon^{\alpha-1} |\lambda_k|^\alpha + \frac{\beta}{\varepsilon} |A|^{2\sigma} \right) + \mathcal{O}(\omega^3 \tau^2). \tag{2.26}$$

**Remark 2.1** (CNFS: Dispersion Relation). The CNFS method (2.18)–(2.19) does not preserve the exact dispersion relation of the plane wave solution, but it gives a good approximation to the dispersion relation if  $\max\{\omega \tau, \omega^3 \tau^2\}$  is small.

### 2.3. Relaxation Fourier spectral method

In [24], a relaxation method was first introduced for the standard NLS, in which the nonlinear part of the NLS is solved in two steps. It shows that the relaxation method is more efficient than the Crank–Nicolson method, if the finite difference or finite element methods are used for spatial discretization [24]. However, if the Fourier spectral method is used for spatial discretization, the relaxation method has the same computational costs as the Crank–Nicolson method.

First, we write the fractional NLS (2.1) as a system of two equations:

$$\begin{aligned} i\varepsilon \partial_t u(x, t) &= \varepsilon^\alpha (-\Delta)^{\alpha/2} u(x, t) + \beta \varphi(x, t) u(x, t), \\ \varphi(x, t) &= |u(x, t)|^{2\sigma}. \end{aligned}$$

Then, the relaxation Fourier spectral (ReFS) method for (2.1) is given by:

$$i \frac{\varepsilon}{\tau} (u_j^{n+1} - u_j^n) = \frac{\varepsilon^\alpha}{2} \left( \delta_x^\alpha U^{n+1} \Big|_j + \delta_x^\alpha U^n \Big|_j \right) + \frac{\beta}{2} (u_j^{n+1} + u_j^n) \varphi_j^{n+\frac{1}{2}}, \tag{2.27}$$

$$\frac{1}{2} (\varphi_j^{n+\frac{1}{2}} + \varphi_j^{n-\frac{1}{2}}) = |u_j^n|^{2\sigma}, \quad 0 \leq j \leq J - 1, \quad n \geq 0, \tag{2.28}$$

where the operator  $\delta_x^\alpha$  is defined in (2.17). At  $n = 0$ , the initial condition is discretized as

$$u_j^0 = \psi(x_j), \quad \varphi_j^{-\frac{1}{2}} = |u_j^0|^{2\sigma} = |\psi(x_j)|^{2\sigma}, \quad 0 \leq j \leq J. \tag{2.29}$$

The ReFS method (2.27)–(2.29) is implicit, and thus at each time step numerical iterations are needed to solve the nonlinear system. It is easy to show that the ReFS method is time reversible. When  $\sigma = 1$ , the ReFS method has both mass and energy conservation in the following lemmas:

**Lemma 2.5** (ReFS: Mass Conservation). *Suppose that  $U^n$  is the numerical solution of the fractional NLS at time  $t_n$ , obtained from the ReFS method in (2.27)–(2.29) with  $\sigma = 1$ . Then, we have the discrete mass*

$$N^n = h \sum_{j=0}^{J-1} |u_j^n|^2 = h \sum_{j=0}^{J-1} |u_j^0|^2 \equiv N^0, \quad n \geq 0. \tag{2.30}$$

**Proof.** Multiplying  $(u_j^{n+1} + u_j^n)^*$  to (2.27) and summing it up for  $0 \leq j \leq J - 1$ , we obtain

$$i \frac{\varepsilon}{\tau} \sum_{j=0}^{J-1} (u_j^{n+1} - u_j^n)(u_j^{n+1} + u_j^n)^* = \sum_{j=0}^{J-1} \left( \frac{\beta}{2} |u_j^{n+1} + u_j^n|^2 \varphi_j^{n+\frac{1}{2}} + \frac{\varepsilon^\alpha (u_j^{n+1} + u_j^n)^*}{2} \sum_{l=-J/2}^{J/2-1} |\mu_l|^\alpha (\widehat{u}_l^{n+1} + \widehat{u}_l^n) \exp(i\mu_l x_j) \right).$$

Taking its imaginary part, and noticing that (2.22) and the function  $\varphi$  is real, we obtain

$$\sum_{j=0}^{J-1} (|u_j^{n+1}|^2 - |u_j^n|^2) = 0,$$

which implies that  $N^{n+1} = N^n$  and thus (2.30), as  $n \geq 0$  is arbitrary.  $\square$

**Lemma 2.6** (ReFS: Energy Conservation). *Suppose that  $U^n$  is the numerical solution of the fractional NLS at time  $t_n$ , obtained from the ReFS method in (2.27)–(2.29) with  $\sigma = 1$ . Then, we have the discrete energy*

$$E^n = h \sum_{j=0}^{J-1} \left[ \varepsilon^\alpha \sum_{l=-J/2}^{J/2-1} |\mu_l|^\alpha |\widehat{u}_l^n|^2 + \beta |u_j^n|^2 \varphi_j^{n-\frac{1}{2}} - \frac{\beta}{2} (\varphi_j^{n-\frac{1}{2}})^2 \right] \equiv E^0, \tag{2.31}$$

for any  $n \geq 0$ .

**Proof.** On the one hand, multiplying  $(u_j^{n+1} - u_j^n)^*$  to (2.27) and summing it up for  $0 \leq j \leq J - 1$ , we get

$$i \frac{\varepsilon}{\tau} \sum_{j=0}^{J-1} |u_j^{n+1} - u_j^n|^2 = \sum_{j=0}^{J-1} \left( \frac{\varepsilon^\alpha (u_j^{n+1} - u_j^n)^*}{2} \sum_{l=-J/2}^{J/2-1} |\mu_l|^\alpha (\widehat{u}_l^n + \widehat{u}_l^{n+1}) \exp(i\mu_l x_j) + \frac{\beta}{2} (u_j^{n+1} + u_j^n)(u_j^{n+1} - u_j^n)^* \varphi_j^{n+\frac{1}{2}} \right).$$

Taking its real part yields

$$\sum_{j=0}^{J-1} \left( \frac{\varepsilon^\alpha}{2} \sum_{l=-J/2}^{J/2-1} |\mu_l|^\alpha (|\widehat{u}_l^{n+1}|^2 - |\widehat{u}_l^n|^2) + \frac{\beta}{2} (|u_j^{n+1}|^2 - |u_j^n|^2) \varphi_j^{n+\frac{1}{2}} \right) = 0.$$

On the other hand, multiplying  $(\varphi_j^{n+\frac{1}{2}} - \varphi_j^{n-\frac{1}{2}})$  to (2.28) with  $\sigma = 1$  and summing it from 0 to  $n$ , we obtain

$$\begin{aligned} \frac{1}{2} \left( (\varphi_j^{n+\frac{1}{2}})^2 - (\varphi_j^{n-\frac{1}{2}})^2 \right) &= \sum_{m=0}^n |u_j^m|^2 (\varphi_j^{m+\frac{1}{2}} - \varphi_j^{m-\frac{1}{2}}) \\ &= \sum_{m=0}^n (|u_j^m|^2 - |u_j^{m+1}|^2) \varphi_j^{m+\frac{1}{2}} - |u_j^0|^2 \varphi_j^{-\frac{1}{2}} + |u_j^{n+1}|^2 \varphi_j^{n+\frac{1}{2}}. \end{aligned}$$

Combining the above two equations leads to

$$\sum_{j=0}^{J-1} \left[ \varepsilon^\alpha \sum_{l=-J/2}^{J/2-1} |\mu_l|^\alpha |\widehat{u}_l^{n+1}|^2 + \beta |u_j^{n+1}|^2 \varphi_j^{n+\frac{1}{2}} - \frac{\beta}{2} (\varphi_j^{n+\frac{1}{2}})^2 \right] = \sum_{j=0}^{J-1} \left[ \varepsilon^\alpha \sum_{l=-J/2}^{J/2-1} |\mu_l|^\alpha |\widehat{u}_l^0|^2 + \beta |u_j^0|^2 \varphi_j^{-\frac{1}{2}} - \frac{\beta}{2} (\varphi_j^{-\frac{1}{2}})^2 \right],$$

for any  $n \geq 0$ , which implying the energy conservation in (2.31).  $\square$

Assume that at time  $t = t_n$  (for any  $n \geq 0$ ), the solution  $u_j^n$  is a plane wave solution of the form in (2.14). Then, we find that the time frequency  $\omega$  obtained from the ReFS method (2.27)–(2.29) satisfies (2.26).

**Table 1**

The values of mass  $N(t)$  at different time  $t$  in solving the 1D fractional NLS (2.1) with  $\varepsilon = 1, \alpha = 1.5, \sigma = 1$  and  $\beta = 2$ , where the initial condition is (3.1).

Time	SSFS	CNFS	ReFS
$t = 0$	6.3813600776042669	6.3813600776042669	6.3813600776042669
$t = 2$	6.3813600776043637	6.3813600776041390	6.3813600776043593
$t = 4$	6.3813600776044765	6.3813600776040227	6.3813600776044428
$t = 6$	6.3813600776046160	6.3813600776038797	6.3813600776045032
$t = 8$	6.3813600776046577	6.3813600776037678	6.3813600776045503
$t = 10$	6.3813600776047359	6.3813600776036479	6.3813600776046275

**Table 2**

The values of energy  $E(t)$  at different time  $t$  in solving the 1D fractional NLS (2.1) with  $\varepsilon = 1, \alpha = 1.5, \sigma = 1$  and  $\beta = 2$ , where the initial condition is (3.1).

Time	SSFS	CNFS	ReFS
$t = 0$	57.432240698438406	57.432240698438406	57.432240698438406
$t = 2$	57.432240698439358	57.432240698437134	57.432240698439315
$t = 4$	57.432240698440559	57.432240698436004	57.432240698440161
$t = 6$	57.432240698441866	57.432240698434526	57.432240698440765
$t = 8$	57.432240698442264	57.432240698433425	57.432240698441248
$t = 10$	57.432240698443110	57.432240698432238	57.432240698442030

**Remark 2.2** (ReFS: dispersion Relation). The ReFS method (2.27)–(2.19) does not preserve the exact dispersion relation of the plane wave solution, but it gives a good approximation to the dispersion relation if  $\max\{\omega\tau, \omega^3\tau^2\}$  is small.

### 3. Numerical experiments

In this section, we apply the numerical methods in Section 2 to study the plane wave solutions and soliton dynamics of the fractional NLS. The accuracy and performance of the SSFS, CNFS and ReFS methods are tested and compared in different cases. For the CNFS and ReFS methods, the fixed point iteration method is used to solve the nonlinear system at each time step.

#### 3.1. Plane wave dynamics

The dynamics of the plane wave solutions in the fractional NLS have been recently investigated in [15]. It shows that due to the nonlocality of the fractional Laplacian  $-(-\Delta)^{\alpha/2}$ , the stability and dynamics of the plane wave solution in the fractional NLS are significantly different from that in the standard NLS. Here, we will focus on testing the performance of the SSFS, CNFS and ReFS in simulating the plane wave dynamics of the one-dimension (1D) fractional NLS.

**Example 1.** We study the plane wave solutions of the 1D fractional NLS (1.1) on a finite domain  $[-\pi, \pi]$ . The parameters are chosen as  $\varepsilon = 1, \sigma = 1$ , and  $\beta = 2$ , and the initial condition is taken as

$$u(x, 0) = \exp(i4x), \quad x \in [-\pi, \pi], \tag{3.1}$$

i.e., the amplitude  $A = 1$  and the wave number  $\lambda_k = 4$ . It is easy to verify that the exact solution of (1.1) with (3.1) is

$$u(x, t) = \exp[i(4x - \omega t)], \quad \text{with } \omega = |\lambda_k|^\alpha + \beta|A|^2 = 4^\alpha + 2. \tag{3.2}$$

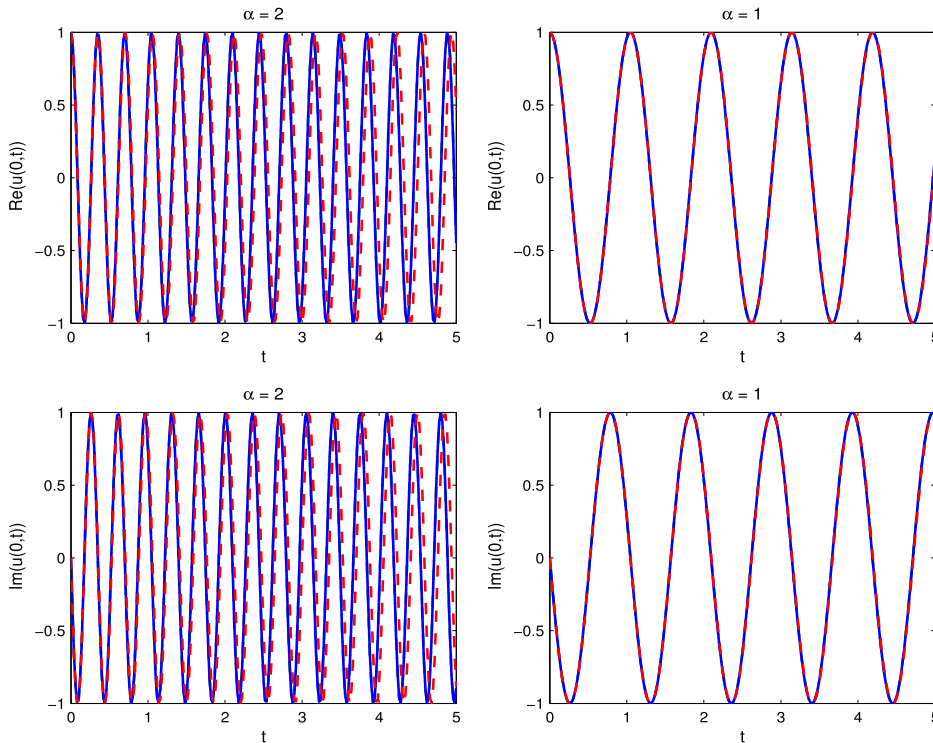
In our simulations, we choose the mesh size  $h = \pi/32$  and the time step  $\tau = 0.02$ .

Table 1 presents the values of mass  $N(t)$  of the SSFS, CNFS and ReFS methods at different time  $t$ , where the fractional power  $\alpha = 1.5$ ; Table 2 displays the corresponding energy  $E(t)$ . It shows that all of these three methods preserve the mass of the fractional NLS, which is consistent with our analytical results in Section 2. Table 2 shows that both the CNFS and ReFS methods have the energy conservation, which verifies our analysis in Lemmas 2.4 and 2.6. In addition, the SSFS preserves the energy well in solving the plane wave solution, although it is not analytically proved.

As discussed in Lemma 2.2, the SSFS method exactly preserves the dispersion relation of the plane wave solutions, if the numerical errors are insignificant. In contrast, Remarks 2.1 and 2.2 show that the CNFS and ReFS methods have a good approximation to the dispersion relation only when  $\max\{\omega\tau, \omega^3\tau^2\} \ll 1$ . To illustrate this difference, let us focus on the solution at  $x = 0$  and study the time evolution of  $\text{Re}(u(0, t))$  and  $\text{Im}(u(0, t))$ . Substituting  $x = 0$  in (3.2), we obtain the exact solution:

$$\text{Re}(u_{\text{exact}}(0, t)) = \cos(\omega t), \quad \text{Im}(u_{\text{exact}}(0, t)) = -\sin(\omega t), \tag{3.3}$$

i.e., they are periodic functions with  $\omega$  in (3.2) defining the frequency. If the numerical solution preserves the dispersion relation, it should have the same time frequency as  $\omega$  in the exact solution.



**Fig. 1.** Time evolution of  $\text{Re}(u(0, t))$  and  $\text{Im}(u(0, t))$  from the exact solution (3.3) (dashed dot line), the SSFS method (solid line) and the CNFS method (dashed line). Note that the graphs of the exact solution and the numerical solution from the SSFS method are identical.

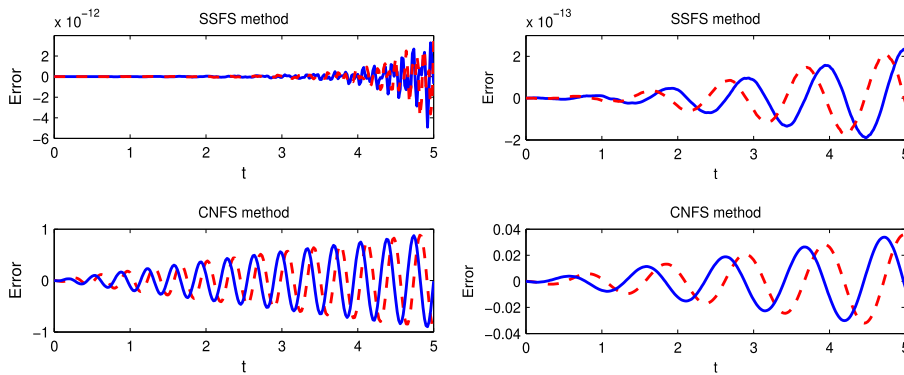


**Fig. 2.** Numerical errors in  $\text{Re}(u(0, t))$  (solid line) and  $\text{Im}(u(0, t))$  (dashed line) of the SSFS and CNFS methods, where  $\alpha = 2$  (left) or  $\alpha = 1$  (right).

In Fig. 1, we present the time evolution of  $\text{Re}(u(0, t))$  and  $\text{Im}(u(0, t))$  computed from the SSFS and CNFS methods, for  $\alpha = 1$  or 2. Note that the results from the ReFS and CNFS methods are almost the same; thus for a better illustration, we omit the results of the ReFS method from Fig. 1. It shows that the graphs of the exact solution and the numerical solution from the SSFS method are the same, independent of the power  $\alpha$ , which suggests that the SSFS method preserves the exact time frequency of the plane wave solution. However, the solution from the CNFS method is more accurate when the power  $\alpha$  is small or the time  $t$  is short, since it does not exactly satisfy the dispersion relation. For example, when  $\alpha = 2$ , the numerical solution from the CNFS method has almost the same time frequency as the exact solution in a short time, but their difference becomes significant over time. While  $\alpha = 1$ , the results from the CNFS method are consistent with the exact solution for a longer time. In fact, when  $\omega\tau$  is small, the error of the CNFS method in approximating the dispersion relation is  $\mathcal{O}(\omega^3\tau^2)$ ; see (2.26). Here, we have  $\omega^3\tau^2 = 2.3328$  for  $\alpha = 2$ , while 0.0864 for  $\alpha = 1$ . Hence, the CNFS method gives a better approximation to the dispersion relation (reflected by the time frequency) for  $\alpha = 1$ .

To further illustrate it, we present the numerical errors in  $\text{Re}(u(0, t))$  and  $\text{Im}(u(0, t))$  of the SSFS and CNFS methods in Fig. 2. It shows that for both SSFS and CNFS methods, the smaller the fractional power  $\alpha$ , the smaller the numerical errors in the dispersion relation. We remark that the errors of the SSFS method increase over time due to the accumulation of numerical errors. For the same power  $\alpha$ , the numerical errors from the CNFS method are much larger than those from

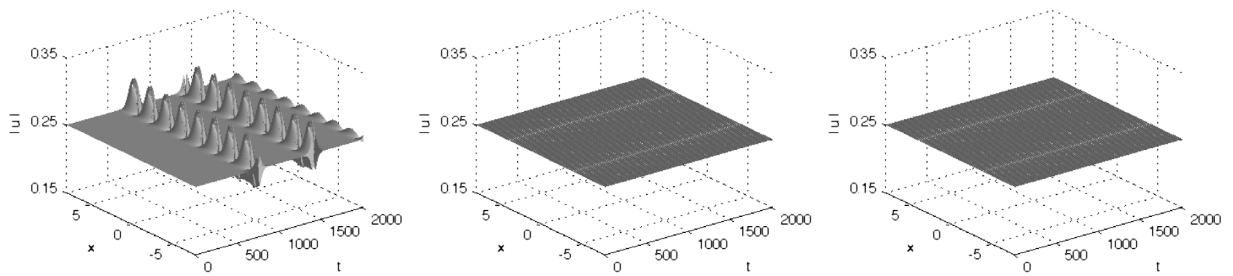


**Fig. 3.** Time evolution of  $|u(x, t)|$  computed by the SSFS (left), CNFS (middle), and ReFS (right) methods, where  $\varepsilon = 1$ ,  $\alpha = 1.1$ ,  $\sigma = 1$  and  $\beta = -1$  in the 1D fractional NLS (1.1) with the initial condition (3.4) and  $h = 5\pi/1024$  and  $\tau = 0.00909$ . It shows that the SSFS method is numerically unstable.

the SSFS method, which is mainly because the solutions of the CNFS method have different frequency from the analytical solution, i.e., the CNFS method does not satisfy the analytical dispersion relation. Our extensive simulations show that the numerical errors of the CNFS and ReFS methods can be significantly reduced by decreasing the time step  $\tau$  and consequently reducing  $\omega^3\tau^2$ .

**Example 2.** We further compare the performance of the SSFS, CNFS and ReFS methods in simulating the plane wave solutions. Here, we consider the fractional NLS (1.1) on a finite domain  $[-2.5\pi, 2.5\pi]$  with  $\varepsilon = 1$ ,  $\alpha = 1.1$ ,  $\sigma = 1$  and  $\beta = -1$ . The initial condition is chosen as the plane wave solution with a small perturbation [15], i.e.,

$$u(x, 0) = \frac{1}{4}[1 + \delta_0 \cos(x/5)], \quad -2.5\pi \leq x \leq 2.5\pi, \quad (3.4)$$

with  $|\delta_0| \ll 1$ . In our simulations, we choose  $\delta_0 = 10^{-5}$ . The mesh size is chosen as  $h = 5\pi/1024$ . It shows that the SSFS method might introduce numerical instability in simulating the plane wave solution of the NLS, and one sufficient condition to ensure its stability is that the mesh size and time step satisfies  $\tau < h^\alpha/\pi^{\alpha-1}$  for  $\alpha \in (0, 2]$ ; see [15] for more discussions. In contrast, the CNFS and ReFS methods allow much larger time step  $\tau$  in the simulations.

To illustrate this, we choose the time step  $\tau = 0.00909$ , larger than the stability threshold ( $\tau = 0.009$ ) of the SSFS method, and simulate the plane wave dynamics by the SSFS, CNFS and ReFS methods. Fig. 3 presents the time evolution of the density  $|u(x, t)|$  computed from the SSFS, CNFS and ReFS methods. It shows that many humps appear in the solution of the SSFS method because of its numerical instability. However, due to the mass conservation of the SSFS method, this instability does not grow unboundedly, and the plane wave solution recurs periodically. By contrast, the plane wave solution from the CNFS and ReFS methods remain stable (see Fig. 3 middle and right panels).

In summary, as implicit numerical methods, the CNFS and ReFS methods are more stable, but they do not preserve the exact dispersion relation of the plane wave solution. Hence, the SSFS method is more accurate and efficient in simulating the plane wave dynamics of the fractional NLS, especially when the frequency  $\omega$  is large.

### 3.2. Soliton dynamics

Soliton is one important type of solution of the NLS. The properties of solitons in the standard NLS have been well studied. In contrast, the results of solitons in the fractional NLS is still very limited. Recently, the dynamics of solitons in the fractional NLS have been reported, and the decoherence of solitons is observed in the presence of a harmonic potential [19].

**Example 3.** We study the dynamics of soliton solutions in the 1D fractional NLS (1.1) with  $\varepsilon = 1$ ,  $\sigma = 1$ , and  $\beta = -2$ . The initial condition is chosen as

$$u(x, 0) = 2 \operatorname{sech}(x), \quad x \in \mathbb{R}. \quad (3.5)$$

For  $\alpha = 2$ , the exact solution is a breather solution given by

$$u(x, t) = 4 \exp(it) \frac{\cosh(3x) + 3 \cosh(x) \exp(i8t)}{\cosh(4x) + 4 \cosh(2x) + 3 \cos(8t)}. \quad (3.6)$$

However, the exact solution of (1.1) with (3.5) still remains unknown for  $\alpha \in (0, 2)$ . In our simulations, we choose the computational domain as  $[-20, 20]$  with the mesh size  $h = 5/1024$ .

Fig. 4 shows the time evolution of the density  $|u(x, t)|$  of the NLS with different power  $\alpha$ . Note that the results from the SSFS, CNFS and ReFS methods are almost the same, and here we present the results from the SSFS method. In the standard NLS with  $\alpha = 2$ , the time evolution of breather solution is periodic, consistent with the analytical result in (3.6). In the fractional NLS, the emergence of the breather becomes more frequent, and the solution is more concentrated at the center of the domain (i.e.,  $x = 0$ ). Moreover, the radiation of waves is observed during the dynamics. The smaller the fractional power

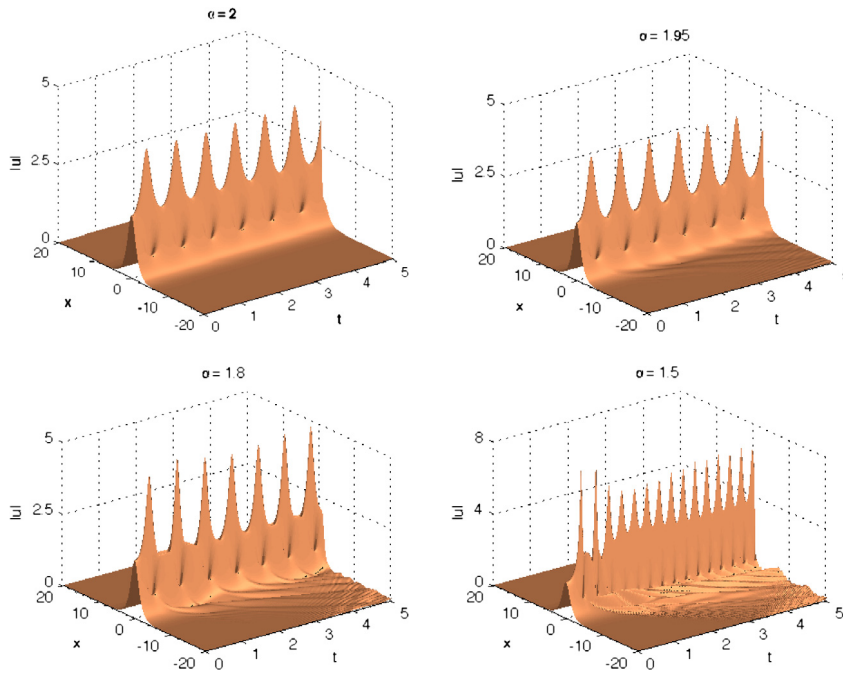


Fig. 4. Time evolution of the density  $|u(x, t)|$  in the NLS (1.1) with the initial condition (3.5), where  $\varepsilon = 1, \sigma = 1$  and  $\beta = -2$ .

Table 3

The value of mass  $N(t)$  at different time  $t$  in solving the 1D fractional NLS (1.1) with  $\varepsilon = 1, \alpha = 1.8, \sigma = 1$  and  $\beta = -2$ , where the initial condition is (3.5).

Time	SSFS	CNFS	ReFS
$t = 0$	7.9999999999999458	7.9999999999999458	7.9999999999999458
$t = 2$	8.0000000002765894	8.0000000000006217	8.0000000000006271
$t = 4$	8.0000091839970597	8.0000000000011227	8.0000000000011600
$t = 6$	8.0001297122930115	8.0000000000017586	8.0000000000018296
$t = 8$	8.0000531725501371	8.0000000000022844	8.0000000000024585
$t = 10$	8.0001549778928691	8.0000000000028741	8.0000000000030962

Table 4

The value of energy  $E(t)$  at different time  $t$  in solving the 1D fractional NLS (1.1) with  $\varepsilon = 1, \alpha = 1.8, \sigma = 1$  and  $\beta = -2$ , where the initial condition is (3.5).

Time	SSFS	CNFS	ReFS
$t = 0$	-18.596224291369765	-18.596224291369744	-18.596224291369683
$t = 2$	-18.597011018365492	-18.596224291375389	-18.596224291376448
$t = 4$	-18.603007342537495	-18.596224291380352	-18.596224291380835
$t = 6$	-18.596334628150188	-18.596224291387063	-18.596224291387987
$t = 8$	-18.596407670783982	-18.596224291392677	-18.596224291394449
$t = 10$	-18.597918856017230	-18.596224291399118	-18.596224291400866

$\alpha$ , the more frequent the breather appears, the stronger the radiation of waves. This suggests that numerical simulations for the fractional NLS are more challenging than for the standard NLS. The blow up of solutions is observed when  $\alpha$  is too small.

Tables 3 and 4 present the mass and energy of the three methods at different time  $t$ , where the power  $\alpha = 1.8$  and the time step  $\tau = 0.001$ . Even though it is proved that all of these three methods are mass conserved, Table 3 shows that the CNFS and ReFS methods have a better conservation than the SSFS method. Table 4 shows the energies of the CNFS and ReFS methods are also conserved, verifying our analytical results in Lemmas 2.4 and 2.6. The energy of the SSFS method oscillates around its initial value.

Next, we study the temporal accuracy of the SSFS, CNFS and ReFS methods. To this end, we use a small mesh size  $h = 5/1024$  in all simulations, such that the errors from spatial discretization is negligible comparing to those from temporal discretization. For a fixed  $\alpha$ , the “exact” solution  $u(t)$  is numerically obtained by using a small time step  $\tau = 10^{-5}$ . Let  $u^{h,\tau}(t)$  denote the numerical solution obtained using the mesh size  $h$  and time step  $\tau$ . Fig. 5 presents the numerical errors  $\|u(t) - u^{h,\tau}(t)\|_2$  at time  $t = 1$  for different  $\alpha$ . It shows that for each  $\alpha$ , all of these three methods have the second-order temporal accuracy, but the numerical errors of the CNFS and ReFS methods are usually smaller than those from the SSFS

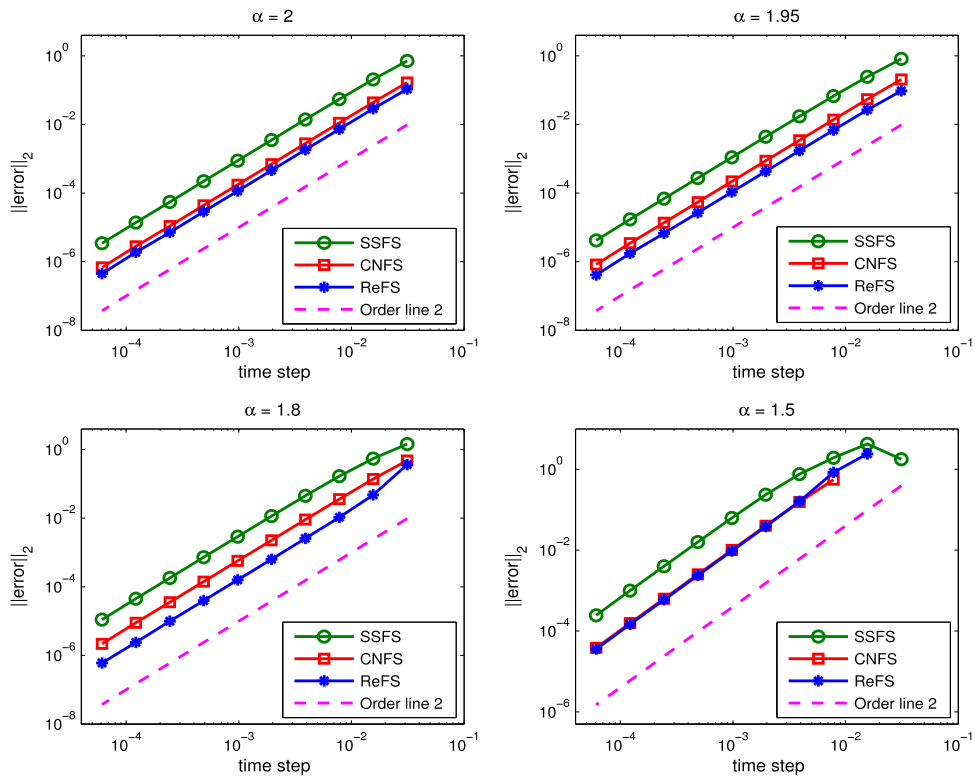


**Fig. 5.** Temporal accuracy of the SSFS, CNFS and ReFS methods in solving the 1D fractional NLS (1.1) with  $\varepsilon = 1$ ,  $\sigma = 1$ , and  $\beta = -2$ , where the initial condition is (3.5).

method. In particular, when  $\alpha$  is close to 2, the ReFS method has a better accuracy than both of the CNFS and SSFS methods. For each method, if the time step  $\tau$  is fixed, the smaller the fractional power  $\alpha$ , the larger the numerical errors. Hence, a smaller time step is needed as  $\alpha$  decreases in the fractional NLS.

### 3.3. Solutions of the semiclassical fractional NLS

In this section, we test the performance of our numerical methods in solving the semiclassical fractional NLS (1.1) with  $\varepsilon = 0.1$  and  $\sigma = 1$ . As the semiclassical parameter  $\varepsilon \rightarrow 0$ , the numerical simulations of the NLS become considerably challenging [25,10]. In our simulations, the initial condition is chosen as a soliton of the form:

$$u_0(x) = \operatorname{sech}(x). \tag{3.7}$$

The computational domain is chosen as  $[-20, 20]$  with mesh size  $h = 5/2048$ . Then, we study the dynamics of both the focusing and defocusing NLS.

**Example 4 (Focusing NLS).** We first study the soliton dynamics in the focusing NLS with  $\beta = -1$ . Fig. 6 shows the time evolution of  $|u(x, t)|$  for various  $\alpha$ . Initially, the modulus of the solution  $|u(x, t)|$  grows over time. At around  $t = 0.5$ , the soliton reaches its maximum height; then the decoherence of the solution starts, and the soliton splits into smaller peaks over time. It shows that the decoherence is stronger for a smaller  $\alpha$ . As  $\alpha$  decreases, the nonlocal effect of the fractional Laplacian  $-(-\Delta)^{\alpha/2}$  becomes stronger, and the maximum peak always occurs at the center of the domain (see Fig. 6 for  $\alpha = 1.5$ ).

Fig. 7 presents the temporal errors  $\|u(t) - u^{h,\tau}(t)\|_{l^2}$  versus the time step  $\tau$  at time  $t = 0.5$ , where the “exact” solution  $u(t)$  is computed by using a small time step  $\tau = 10^{-5}$ . It shows that all the three methods have the second-order temporal accuracy in solving the semiclassical fractional NLS, but for fixed  $\alpha$  and  $\tau$ , the CNFS method has the smallest numerical errors among the three methods. For a fixed time step  $\tau$ , the numerical errors of each method increases as the fractional power  $\alpha$  decreases. Comparing Figs. 5 and 7, we find that the numerical errors of the SSFS and ReFS methods increase for a smaller  $\varepsilon$ , but the errors of the CNFS method remain the same order. This implies that the CNFS might be a better method in simulating the focusing fractional NLS in the semiclassical regime.

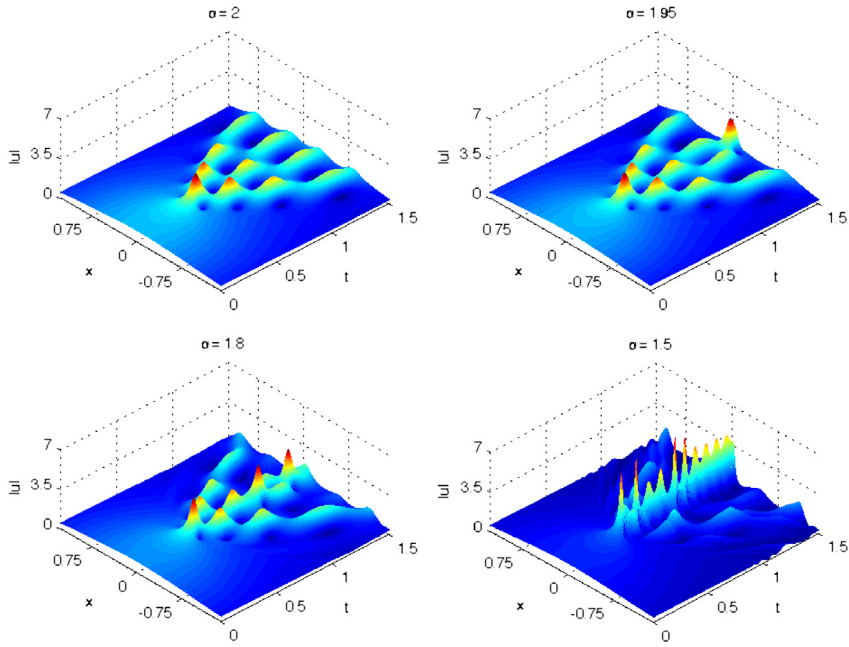


Fig. 6. Time evolution of the density  $|u(x, t)|$  of the semiclassical NLS (1.1) with the initial condition (3.7), where  $\varepsilon = 0.1$ ,  $\sigma = 1$ , and  $\beta = -1$ .

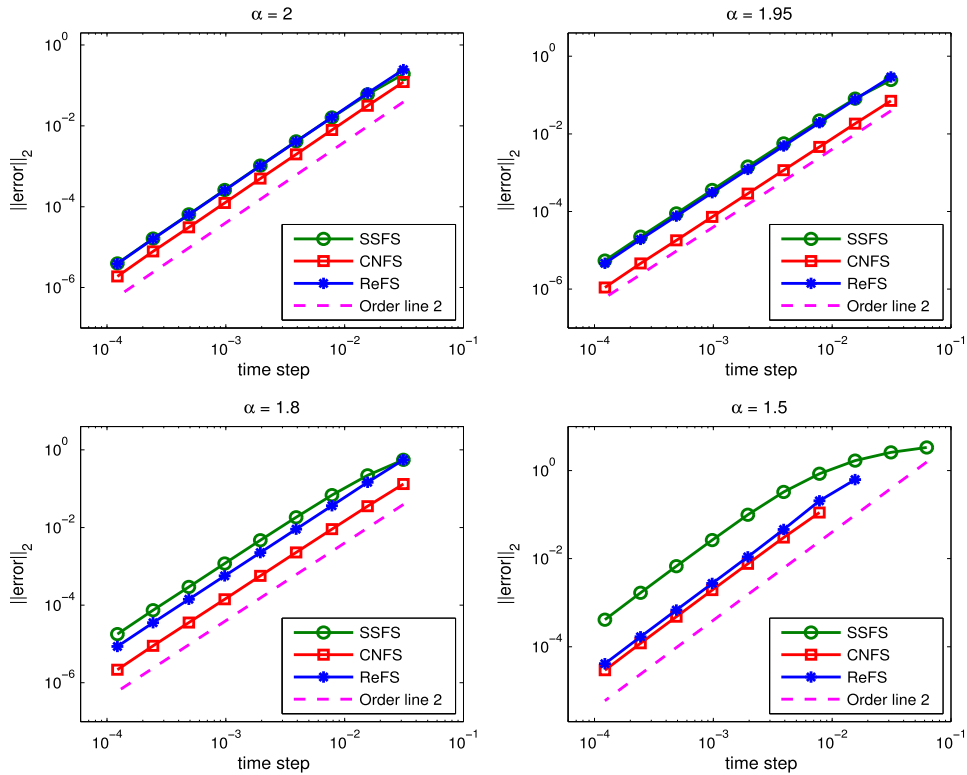


Fig. 7. Temporal accuracy of the SSFS, CNFS and ReFS methods in solving the 1D semiclassical fractional NLS (1.1) with  $\varepsilon = 0.1$ ,  $\sigma = 1$  and  $\beta = -1$ , where the initial condition is (3.7).

**Example 5 (Defocusing NLS).** We move to the dynamics of the defocusing NLS with  $\beta = 1$ . Fig. 8 demonstrates the time evolution of the density  $|u(x, t)|$  for various  $\alpha$ . In contrast to the focusing case, the nonlinear interactions are repulsive in this case. Hence, the dynamics of the solitons are significantly different from those in Fig. 5 for the focusing NLS. Instead of concentrating, the soliton expands over time, creating sharper layers at the edges of the solution. After certain time,

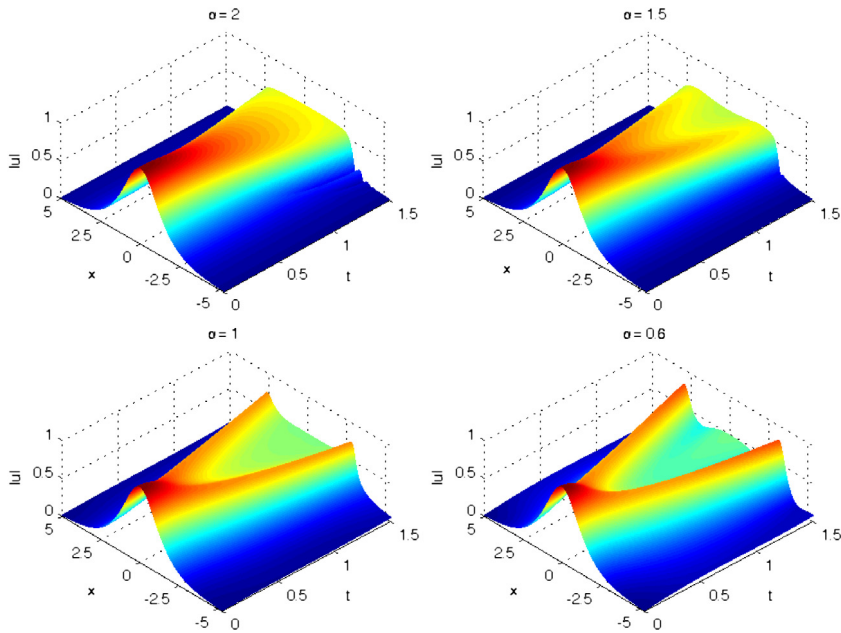


Fig. 8. Time evolution of the density  $|u(x, t)|$  of the semiclassical NLS (1.1) with the initial condition (3.7), where  $\varepsilon = 0.1, \sigma = 1$ , and  $\beta = 1$ .

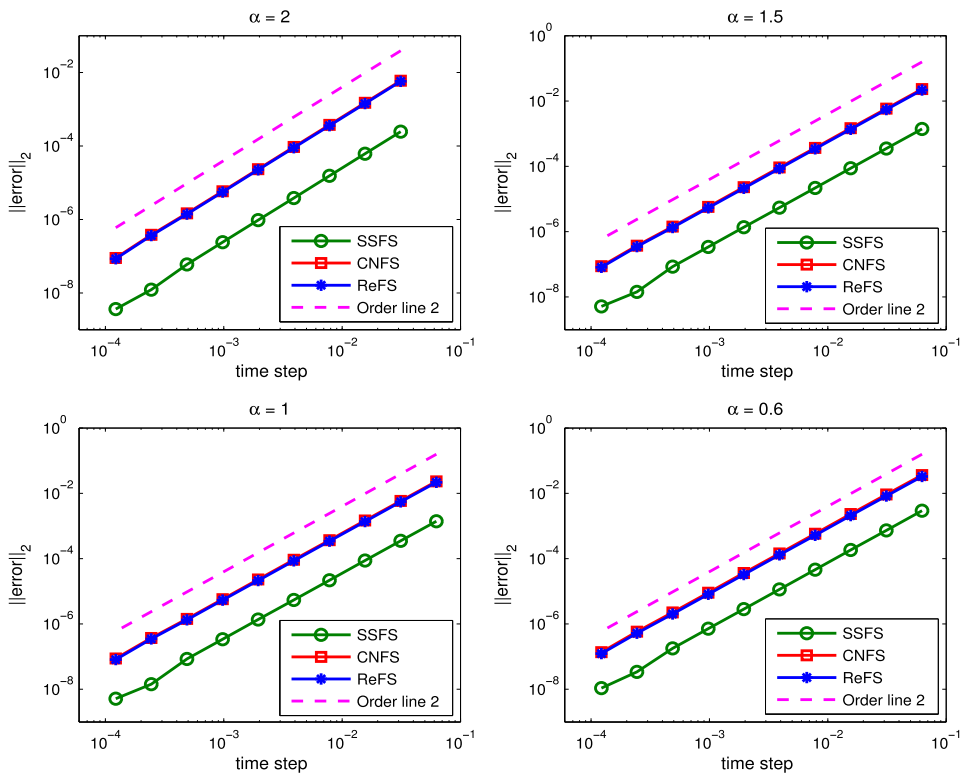


Fig. 9. Temporal accuracy of the SSFS, CNFS and ReFS methods in solving the 1D semiclassical fractional NLS (1.1) with  $\varepsilon = 0.1, \sigma = 1$  and  $\beta = 1$ , where the initial condition is (3.7).

the solution splits into two solitons moving in different directions, and the smaller the fractional power  $\alpha$ , the earlier the solution splits.

Fig. 9 presents the temporal errors  $\|u(t) - u^{h,\tau}(t)\|_2$  versus the time step  $\tau$  at time  $t = 0.5$ , where the “exact” solution  $u(t)$  is computed by using a small time step  $\tau = 10^{-5}$ . It shows that all of the three methods have the second-order accuracy

for the temporal discretization, but for the same  $\alpha$  and  $\tau$ , the SSFS method has much smaller errors than the CNFS and ReFS methods. Moreover, in contrast to the focusing case, the accuracy of each method is less sensitive to the fractional power  $\alpha$ . It suggests that the SSFS method is more accurate and efficient in simulating the defocusing fractional NLS.

#### 4. Conclusions

We proposed three numerical methods, i.e., the split-step Fourier spectral (SSFS), the Crank–Nicolson Fourier spectral (CNFS), and the relaxation Fourier spectral (ReFS) method, for solving the fractional NLS. All of these methods have the spectral order accuracy in space and the second-order accuracy in time, and the temporal accuracy of the SSFS method can be easily improved using a higher order split-step method. The SSFS method is explicit and mass conservative, and it preserves the dispersion relation. In contrast to the SSFS method, the CNFS method is implicit and mass and energy conservative, but it does not preserve the dispersion relation. The ReFS method has similar properties of the CNFS method, but it satisfies the mass and energy conservation only when  $\sigma = 1$ . Since the CNFS and ReFS methods are implicit, their computational costs are higher than the SSFS method. Our numerical experiments suggested that the SSFS method is better in solving the defocusing NLS, but the CNFS and ReFS methods are more effective for the focusing NLS. In addition, the SSFS method is more efficient for studying the long-time behaviors of the plane wave solutions, as it preserves the dispersion relation.

#### References

- [1] N. Laskin, Fractional quantum mechanics and Lévy path integrals, *Phys. Lett. A* 268 (4–6) (2000) 298–305.
- [2] N. Laskin, Fractional Schrödinger equation, *Phys. Rev. E* 66 (5) (2002) 056108.
- [3] K. Kirkpatrick, E. Lenzmann, G. Staffilani, On the continuum limit for discrete NLS with long-range lattice interactions, *Comm. Math. Phys.* 317 (3) (2013) 563–591.
- [4] A.J. Majda, D.W. McLaughlin, E.G. Tabak, A one-dimensional model for dispersive wave turbulence, *J. Nonlinear Sci.* 7 (1) (1997) 9–44.
- [5] Y. Hu, G. Kallianpur, Schrödinger equations with fractional Laplacians, *Appl. Math. Optim.* 42 (3) (2000) 281–290.
- [6] V.E. Zakharov, P. Guyenne, A.N. Pushkarev, F. Dias, Wave turbulence in one-dimensional models, *Physica D* 152/153 (2001) 573–619.
- [7] S. Longhi, Fractional Schrödinger equation in optics, *Opt. Lett.* 40 (6) (2015) 1117–1120.
- [8] S. Secchi, M. Squassina, Soliton dynamics for fractional Schrödinger equations, *Appl. Anal.* 93 (8) (2014) 1702–1729.
- [9] S. Duo, Y. Zhang, Computing the ground and first excited states of the fractional Schrödinger equation in an infinite potential well, *Commun. Comput. Phys.* 18 (2) (2015) 321–350.
- [10] C. Klein, C. Sparber, P. Markowich, Numerical study of fractional nonlinear Schrödinger equations, *Proc. Math. Phys. Eng. Sci.* 470 (2014) 20140364.
- [11] S.G. Samko, A.A. Kilbas, O.I. Marichev, *Fractional Integrals and Derivatives*, Gordon and Breach Science Publishers, Yverdon, 1993.
- [12] K.B. Oldham, J. Spanier, *The Fractional Calculus: Theory and Applications of Differentiation and Integration to Arbitrary Order*, vol. I, Dover, 2006.
- [13] R. Herrmann, *Fractional Calculus: An Introduction for Physicists*, World Scientific Publishing Company, 2011.
- [14] N. Jacob, *Pseudo-differential Operators and Markov Processes*, vol. I, Imperial College Press, 2001.
- [15] S. Duo, T.I. Lakoba, Y. Zhang, Analytical and numerical study of plane wave dynamics in the fractional nonlinear Schrödinger equation, preprint.
- [16] D. Wang, A. Xiao, W. Yang, A linearly implicit conservative difference scheme for the space fractional coupled nonlinear Schrödinger equations, *J. Comput. Phys.* 272 (2014) 644–655.
- [17] P. Wang, C. Huang, An energy conservative difference scheme for the nonlinear fractional Schrödinger equations, *J. Comput. Phys.* 293 (2015) 238–251.
- [18] P. Amore, F.M. Fernández, C.P. Hofmann, R.A. Sáenz, Collocation method for fractional quantum mechanics, *J. Math. Phys.* 51 (12) (2010) 122101.
- [19] K. Kirkpatrick, Y. Zhang, Fractional Schrödinger dynamics and decoherence, preprint.
- [20] W. Bao, S. Jin, P.A. Markowich, Numerical study of time-splitting spectral discretizations of nonlinear Schrödinger equations in the semiclassical regimes, *SIAM J. Sci. Comput.* 25 (1) (2003) 27–64.
- [21] W. Bao, Y. Zhang, Dynamics of the group state and central vortex states in Bose–Einstein condensation, *Math. Models Methods Appl. Sci.* 15 (12) (2005) 1863–1896.
- [22] W. Bao, Q. Du, Y. Zhang, Dynamics of rotating Bose–Einstein condensates and its efficient and accurate numerical computation, *SIAM J. Appl. Math.* 66 (3) (2006) 758–786.
- [23] J.A.C. Weideman, B.M. Herbst, Split-step methods for the solution of the nonlinear Schrödinger equation, *SIAM J. Numer. Anal.* 23 (3) (1986) 485–507.
- [24] C. Besse, A relaxation scheme for the nonlinear Schrödinger equation, *SIAM J. Numer. Anal.* 42 (3) (2004) 934–952.
- [25] S. Jin, P. Markowich, C. Sparber, Mathematical and computational methods for semiclassical Schrödinger equations, *Acta Numer.* 20 (2011) 211–209.